SiNOI and AlGaAs-on-SOI nonlinear circuits for continuum generation in Si photonics

El Dirani, Houssein; Monat, Christelle; Brision, Stephane; Olivier, Nicolas; Jany, Christophe; Letartre, Xavier; Pu, Minhao; Girouard, Peter David; Frandsen, Lars Hagedorn; Semenova, Elizaveta

Total number of authors:
13

Published in:
Proceedings of SPIE

Link to article, DOI:
10.1117/12.2286862

Publication date:
2018

Document Version
Publisher's PDF, also known as Version of record

PROCEEDINGS OF SPIE

SPIEDigitalLibrary.org/conference-proceedings-of-spie

SiNOI and AlGaAs-on-SOI nonlinear circuits for continuum generation in Si photonics

Houssein El Dirani, Christelle Monat, Stéphane Brision, Nicolas Olivier, Christophe Jany, et al.

Houssein El Dirani, Christelle Monat, Stéphane Brision, Nicolas Olivier, Christophe Jany, Xavier Letartre, Minhao Pu, Peter D. Girouard, Lars Hagedorn Frandsen, Elizaveta Semenova, Leif Katsuo Oxenløwe, Kresten Yvind, Corrado Sciancalepore, "SiNOI and AlGaAs-on-SOI nonlinear circuits for continuum generation in Si photonics," Proc. SPIE 10535, Integrated Optics: Devices, Materials, and Technologies XXII, 1053508 (23 February 2018); doi: 10.1117/12.2286862

SPIE.

Event: SPIE OPTO, 2018, San Francisco, California, United States

SiNOI and AlGaAs-on-SOI nonlinear circuits for continuum generation in Si Photonics

Houssein El Dirani[1], Christelle Monat[2], Stéphane Brision[1], Nicolas Olivier[1], Christophe Jany[1], Xavier Letartre[2], Minhao Pu[3], Peter D. Girouard[3], Lars Hagedorn Frandsen[3], Elizaveta Semenova[3], Leif Katsuo Oxenløwe[3], Kresten Yvind[3], and Corrado Sciancalepore[1]

1- CEA-LETI, Minatec, CEA-Grenoble, F-38054, Grenoble, France
2- CNRS, Institut des nanotechnologies de Lyon, Lyon, France
3- DTU Fotonik, Technical University of Denmark, Kgs. Lyngby, Denmark

ABSTRACT

In this communication, we report on the design, fabrication, and testing of Silicon Nitride on Insulator (SiNOI) and Aluminum-Gallium-Arsenide (AlGaAs) on silicon-on-insulator (SOI) nonlinear photonic circuits for continuum generation in Silicon (Si) photonics. As recently demonstrated, the generation of frequency continua and supercontinua can be used to overcome the intrinsic limitations of nowadays silicon photonics notably concerning the heterogeneous integration of III-V on SOI lasers for datacom and telecom applications. By using the Kerr nonlinearity of monolithic silicon nitride and heterointegrated GaAs-based alloys on SOI, the generation of tens or even hundreds of new optical frequencies can be obtained in dispersion tailored waveguides, thus providing an all-optical alternative to the heterointegration of hundreds of standalone III-V on Si lasers. In our work, we present paths to energy-efficient continua generation on silicon photonics circuits. Notably, we demonstrate spectral broadening covering the full C-band via Kerr-based self-phase modulation in SiNOI nanowires featuring full process compatibility with Si photonic devices. Moreover, AlGaAs waveguides are heterointegrated on SOI in order to dramatically reduce (x1/10) thresholds in optical parametric oscillation and in the power required for supercontinuum generation under pulsed pumping. The manufacturing techniques allowing the monolithic co-integration of nonlinear functionalities on existing CMOS-compatible Si photonics for both active and passive components will be shown. Experimental evidence based on self-phase modulation show SiNOI and AlGaAs nanowires capable of generating wide-spanning frequency continua in the C-Band. This will pave the way for low-threshold power-efficient Kerr-based comb- and continuum- sources featuring compatibility with Si photonic integrated circuits (Si-PICs).

Keywords: Complementary metal-oxide-semiconductor (CMOS), nonlinear integrated optics, Kerr-based continuum generation, nanowires, photonic integrated circuits (PICs), silicon nitride (Si_3N_4), and Aluminum gallium arsenide silicon optoelectronics.

I. INTRODUCTION

The limits of copper-based interconnects of standard electronics circuits and systems in present computing nodes and datacenters will be reached because of the staggering growth witnessed during the past decade in the volume of data traffic running through our telecommunication infrastructures. In this way, the capabilities of existent telecom backbones are increasingly more questioned, especially due to social networks platforms as well as the exponential increase in richer multimedia content exchange over the net. Furthermore, the heat management proves harder and costs for cooling systems are ballooning in present datacenters architectures while shrinking more and more microelectronics nodes as a solution. Therewith, shrinking microelectronics puts at risk its technological viability, as the pin/interconnects density is limited by the shrinking available space over rack and board areas.

Within such situation, the emerging solution of adopting power-efficient broadband optical interconnects capable to face up the mounting demand for data transmission bandwidth as well as aiming at increasing computing capabilities has gained momentum in the last 10 years within both research and industrial environments. In detail, the intrinsic capability of light to transport information over large distances at very high data rates/low latency with minor power dissipation can be thus scaled from to rack-level optical links down to card-to-card till chip-to-chip interconnects. This provides solid perspectives for revolutionizing the way we design and conceive nowadays telecommunication systems and servers architectures as well as high-performance computing, triggering the very beginning of a photonics-based computational era.

Silicon-based photonic integrated circuits (Si-PICs) pave the way towards a brand-new optoelectronics featuring a significant integration potential with cost-effective complementary metal-oxide-semiconductor (CMOS) technology and micro-nano-electronics circuits and nodes [1], [2]. Moreover, the high-index contrast of silicon-on-insulator (SOI)

Integrated Optics: Devices, Materials, and Technologies XXII, edited by Sonia M. García-Blanco, Pavel Cheben, Proc. of SPIE Vol. 10535, 1053508 · © 2018 SPIE
"CCC code: 0277-786X/18/$18 · doi: 10.1117/12.2286862

materials allows for the implementation - over small footprints - of optical functions constituting the whole silicon photonics toolbox such as optical resonators and laser integration [3], input/output (I/O) couplers [4], high-speed modulators [5], Si-Ge photodiodes [6], as well as filters and wavelength (de)multiplexers [7], [8].
However, a footprint bottleneck is coming toward the effort in massively heterointegrating III-V lasers on Silicon for generating on-chip multiple-wavelength optical signals. Specifically, most of the research and development effort was spent in recent years on distributed Bragg reflector (DBR) [9] and DFB-based architectures [10] in order to accomplish data transmission in NRZ or more complex modulation formats for higher aggregate bandwidth capable to provide on-chip light emission to be fed through rings- or Mach-Zehnder-based modulators [11]. Another drawback is the power consumption of the optical link in pJ per transmitted bit. To feed modulators which can run up to 50-60 Gbps, more than 350 mW of both electrical DC and RF powers are in fact necessary solely to operate the laser source.
A possible solution is to shrink laser diodes by using micro-disk [12] or vertical-cavity surface-emitting lasers on Si [13, 14], having access to a larger number of wavelengths on which coding information via on-off keying or external modulators, but this technologies is still not mature yet and we are still intrinsically space-limited because it is rather difficult to go down below 40-50 μm between two lasers.

The potential of X^3 nonlinear optical processes to generate frequency continua or combs via optical parametric oscillators (OPOs) as demonstrated in the last years by different groups [15-19] is the best solution for all the aforementioned drawbacks. In this way, tens or even hundreds of optical channels can be generated thus substituting an equal amount for individual laser diodes to be integrated on a chip.
In this work, two materials are presented. First, AlGaAs which was proposed as first platform for nonlinear optics in the telecommunication band and offers the powerful ability to tune its nonlinearity and factor of merit by varying the alloy composition [20]. Second, the silicon nitride which is a CMOS-compatible material with a linear refractive index of 1.98 at 1,550 nm and, due to its larger bandgap, does not suffer from two-photon absorption and the concomitant free-carrier absorption that plague silicon at communications wavelengths [15].

A 660 Tbits/sec has been demonstrated using a continuum generated in an AlGaAs waveguide with external multiplexers and modulators [19]. In this paper we present the cointegration of the AlGaAs on silicon, using molecular bonding [21], thus bridging between the silicon photonics toolbox and the AlGaAs nonlinearity.

Besides, prior works based on stoichiometric Si_3N_4-based OPOs made use of high-temperature annealing (~1200°C) of the nitride film and silica uppercladding used to break N-H bonds otherwise causing absorption in the C-band and destroying its nonlinear functionality. As well as that, substrate preparation made by etching crack-limiting trenches in the SiO_2 undercladding was used to prevent the propagation of tensile strain-related cracks in the nitride film which would deteriorate dramatically the optical quality of the material [22]. Indeed, the use of such technological building blocks would prevent a straightforward integration of such nonlinear circuits on existing Si-based photonics and optoelectronics as, for instance, extreme annealing would destroy the Silicon optical layer underneath along with its functions (modulation, photodetection, etc…).

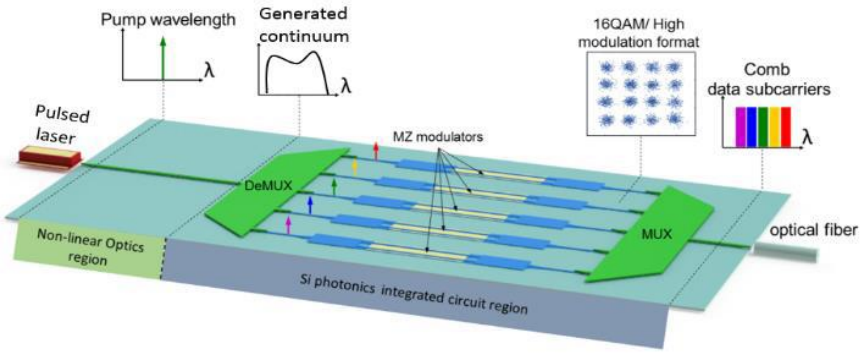

Fig. 1. Principle of ultra-high speed rate communications with Kerr frequency combs. Artistic view of a future ultra-high rate transmitter, leveraging a Kerr frequency continua source onto a Silicon optoelectronic chip including wavelength (de)-multiplexers; Mach-Zehnder modulators, as well as I/O edge- and grating couplers to optical fibers.

In this work, the design, fabrication, and optical testing of a coupler, consisting an AlGaAs waveguide superposed with a silicon waveguide, paving the way for a cointegration of the nonlinear AlGaAs material and silicon photonics toolbox (e.g.

de-multiplexers, modulators), adding a step toward the full integration of on chip transmitter data for ultra-high rate communications.
Also, the design, fabrication and a continuum generation across the C-band of Si_3N_4-based nonlinear circuits by exclusively using technological building blocks which are fully compatible with Si-based optoelectronic circuits previously realized on the wafer carrier [23]. The aim of our work is to pave the way for a comprehensive co-integration of nonlinear continuum generation in nitride-based and AlGaAs circuits to be used as optical seeding of silicon photonic integrated circuits (Si-PICs) for ultra-wideband data communication on a chip.
The paper is organized as follows. In Section II, the architecture, fabrication process, and optical testing of the adiabatic coupler between AlGaAs and Silicon are presented. In Section III, the detailed fabrication process and the continuum generation using a silicon nitride waveguide are presented. Section IV concludes the work and provides readers with perspectives over expected future developments.

II. ALGAAS/SI CO-INTEGRATION AND TESTING

Supermode coupler design

The light propagates in an optical waveguide with different modes depending on the dimension of the waveguide and the wavelength. However, the optical mode with a specific wavelength propagates in a waveguide with a precise effective index. A directional coupler, constituted by two waveguides, imposes a length where the effective index of the coupled mode must be equal. An adiabatic coupler, as in our case, does not depend of the coupler length but just on the effective index of the waveguide mode. In simpler terms, in an adiabatic coupler constituted by two waveguides the light will be where the effective index is bigger. As presented in figure 2 by narrowing the silicon waveguide from 2 um to 120 nm superposed with an AlGaAs waveguide which in his turn is widened from 200 nm to 630 nm, the effectives indices of the fundamental TE-polarized modes at 1550 nm in the two waveguides will cross each other. After the Silicon-to-AlGaAs index-matching point, the light will be almost exclusively in the AlGaAs waveguide where the effective index is bigger as is shown in Fig. 2.

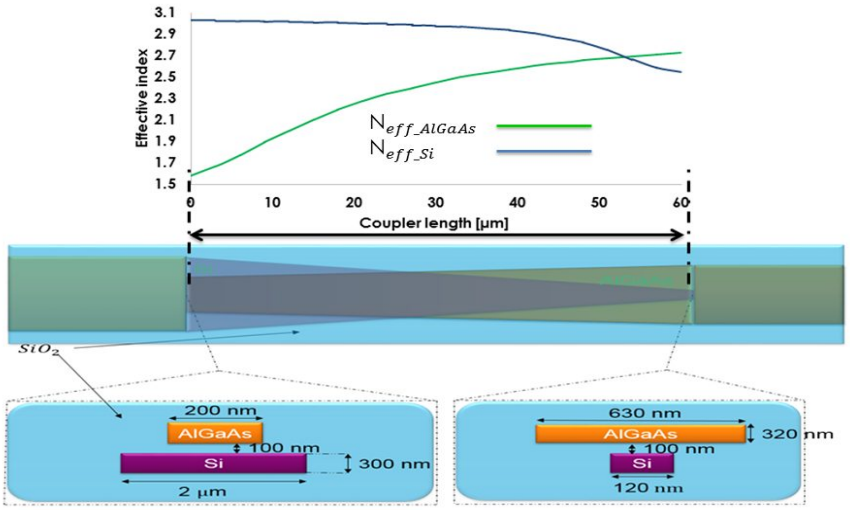

Fig. 2. Si/AlGaAs supermode coupler architecture (a) Top view, beginning and end cross-sections of the supermode coupler architecture. (b) Effectives indices variation in each waveguide in terms of the coupler length.

In order to validate the concept of the adiabatic coupler, a finite differential mode solver has been used to simulate the coupler. As expected the light passes from the silicon to AlGaAs waveguide at the crossing point of the two effective indices. The simulation gives a transmission efficiency of 99 % proving the adiabaticity of the coupler.
In addition, input/output (I/O) edge tapered couplers at the Silicon level were included in order to permit fiber-to-chip optical coupling during optical tests.

AlGaAs/Si co-integration

As presented in figure 2 (a) the waveguides of the coupler are superposed so we have two fabrication stages. The silicon level and the AlGaAs level are presented below separately.

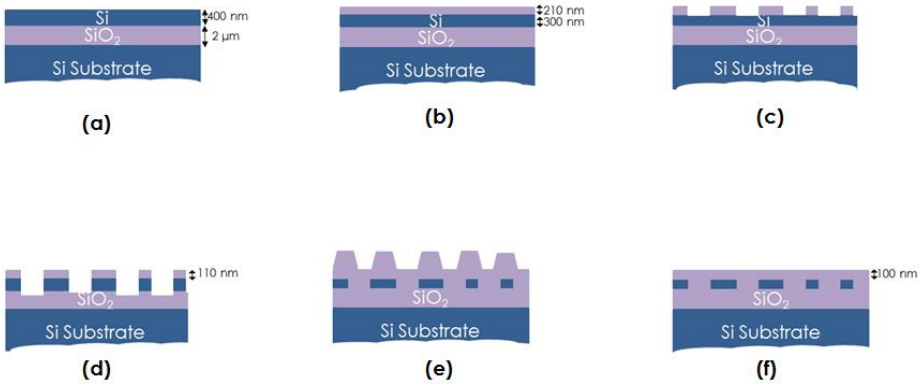

Fig. 3. Cross-section views showing the Si-level fabrication process as detailed in Section II. (a) 400-nm-silicon-layer on 2-um-silica-box SOI wafer (b) Thermal oxidation of the silicon substrate followed by (c) silica dry-etch using DUV resist as hard mask. (d) Silicon layer dry-etch using previously etched silica as hard mask (e) SiO_2 encapsulation by HDP-PECVD (f) chemical mechanical polishing to reduce the layer separating the silicon of the AlGaAs layer. The details of the process flow including processing temperatures, precursors rate flows, etching chemistry and lithography are described in the article text.

The silicon level begin by thermal oxidation of 100 nm of silicon, using an SOITEC SOI wafer with 400 nm of silicon layer and 2 um of box, giving 200 nm of silica which will be used as a hard mask to etch the silicon layer.

Lithography and dry etching technique. Deep-UV (DUV) lithography was performed on a ASML-1100 stepper using 193-nm DUV and 400-nm-thick JSR 1682 resist mask followed by an anti-reflection coating (BARC). In detail, a Ar/Cl2/O2 chemistry was used in a 200-mm reactor. The silicon layer is etched, after stripping the resist, using $HBr/Cl_2/He/O_2$ as etchants.

Encapsulation. Silicon circuits were then encapsulated by plasma-enhanced chemical vapor deposition (PECVD) of a 1-µm-thick SiO_2 cladding layer at 350 °C using SiH_4 and Ar as precursors. The final step in the silicon stage process was a chemical mechanical polishing to reduce the SiO2 layer and keeping just 100 nm constituting the gap between the two Si/AlGaAs waveguides.

A molecular, or covalent bond, is formed when atoms bond by sharing pairs of electrons. This sharing can occur from atom to atom, or from an atom to another molecular bond. In our process, the molecular bonding permitted the co-integration AlGaAs with silicon. This intermediary level began with an annealing for two hours of the silicon wafer in order to outgas the residual hydrogen followed by cleaning. Before bonding the SOI wafer is rinsed and dried. For the Gallium Arsenide wafer, ozone cleaning for 10 min is performed followed by deionized water cleaning.

The bonding process is performed under vacuum bonding machine at 200°C for two hours, while a force of ~750 N is applied to the bonded wafers. Subsequently, the GaAs substrate is removed in two wet etching steps, with a sulfuric acid/hydrogen peroxide solution (H_2SiO_4:H_2O_2 _ 5:4) and slow etch step in a selective citric acid/hydrogen peroxide solution ($C_6H_8O_7$:H_2O_2 _4:1) . After the etch-stop layers (InGaP) was wet etched using hydrochloric acid.

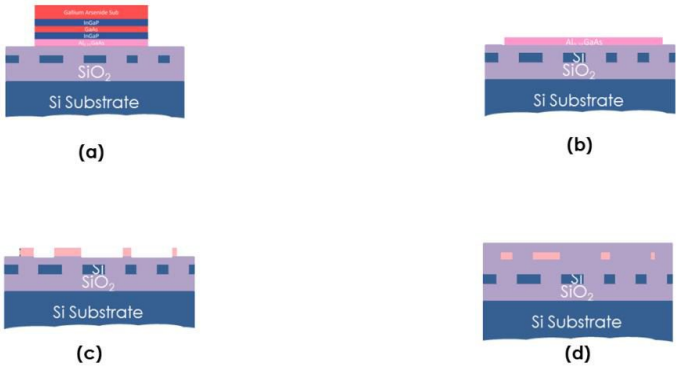

Fig. 4. Cross-section views showing the AlGaAs-level fabrication process as detailed in Section II. (a) AlGaAs wafer bonded on SOI wafer (b) Substrate (GaAs) and etch stop layers (InGaP) removal(c) AlGaAs dry-etch using M78Y DUV resist as hard mask (d) SiO_2 encapsulation by TEOS low stress (f) chemical mechanical polishing to reduce the layer separating the silicon of the AlGaAs layer. The details of the process flow including processing temperatures, precursors rate flows, etching chemistry and lithography are described in the article text.

Lithography and dry etching technique. Deep-UV (DUV) lithography was performed on a ASML-300 stepper using 248-nm DUV and 780-nm-thick M78Y resist mask followed by a 40-nm-thick anti-reflection coating (BARC). Chloride-based dry etching was used to pattern the different architectures on the bonded AlGaAs film using solely the resist as hard mask and the SiO_2 as stop etch layer. In detail, a BCl_3/Cl_2 chemistry was used in a 200-mm reactor. After etching the resist is striped.

Encapsulation. AlGaAs circuits were then encapsulated by 1 µm tetraethoxysilane (TEOS) low stress at T=260 °C and the wafer is finally diced in order to test the supermode coupler.

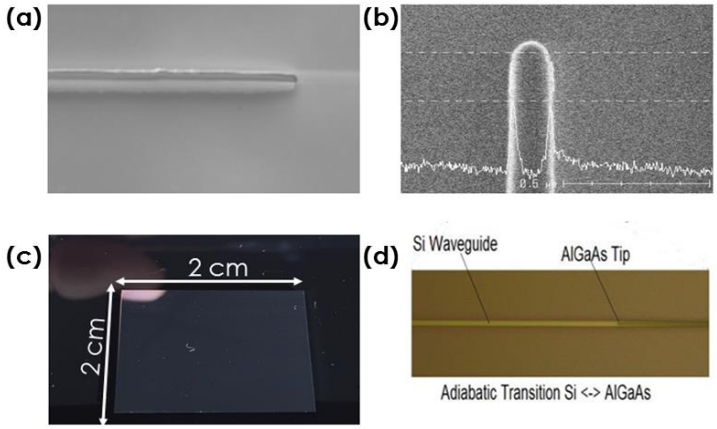

Fig. 5. (a) Focused ion beam image of an 200-nm-AlGaAs tip. (b) Scanning electronic microscope image of an 120-nm-Silicon tip. (c) 2 cm x 2 cm AlGaAs/Si chip ready for test. (d)Optical microscope photo of the AlGaAs and Silicon superposed tapers.

AlGAAs/Si link test

An optical station is used in order to test the coupler using a 2-um-lensed fiber to couple the light into the waveguide. As presented in the figure 6 the light is well coupled into the AlGaAs waveguide. The losses have been deduced by subtracting the propagation losses and the coupling of the whole insertion losses. The transition losses reveal 0.4 dB/transition. We believe that this losses comes from the overlays between the AlGaAs and the Silicon tip which is around 70 nm.

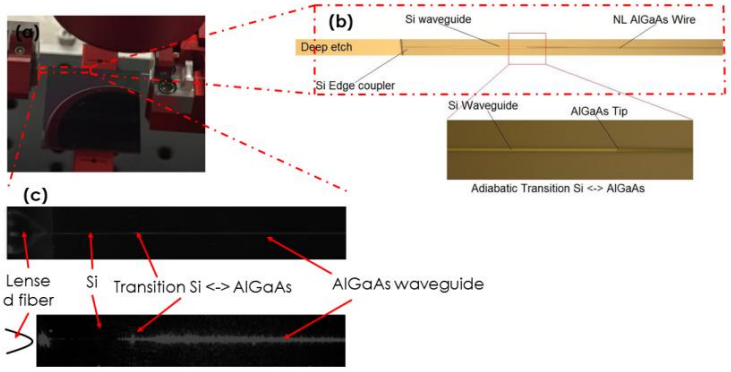

Fig. 6. Si/AlGaAs supermode coupler test (a) optical station with the chip under test (b) Optical microscope image of the AlGaAs and Silicon superposed tapers (c) Infrared image of the Si/AlGaAs coupler featuring the adiabatic transition between the silicon and the AlGaAs waveguide

This link between nonlinear AlGaAs and silicon constitutes and essential building block of the nonlinear AlGaAs material and silicon photonics toolbox (e.g. multiplexer modulators) and approaching a step toward the full integration of on-chip transmitter data for ultra-high rate communications as presented in figure 1.

III. NONLINEAR SI_3N_4 FABRICATION AND TEST

Wideband sources have several applications like spectroscopy and telecommunications. Silicon nitride is an attractive CMOS material for nonlinear wideband source generation because of the absence of two-photon absorption due to a large 3.6-eV bandgap.

The lithographic mask included different critical building blocks each serving a different characterization purpose. In detail, single-mode 750-nm-wide waveguides and waveguides exhibiting anomalous dispersion with a 0-GVD (group velocity dispersion) point set at 1570 nm were used in order to provide for super continuum generation using 720-nm-thick waveguides having their width varying from 1.4-µm- to 1.7-µm in order display anomalous dispersion over a broad spectral range. In addition, input/output (I/O) grating and edge tapered couplers were included in order to permit fiber-to-chip optical coupling during optical tests.

The whole process was based on 200-mm silicon wafers and developed on LETI CMOS pilot lines and is sketched in figure 7(a-d).

Si3N4 circuits fabrication

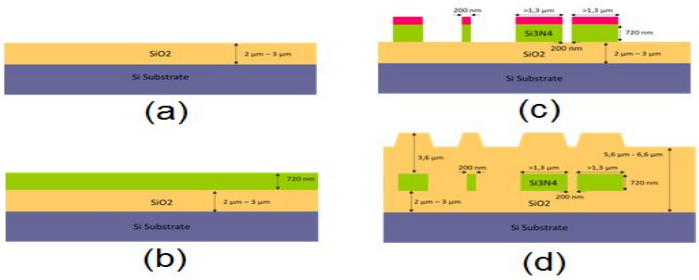

Fig. 7. Cross-section views showing the Si_3N_4 fabrication process as detailed in Section II. (a) Thermal oxidation of the silicon substrate followed by (b) multiple-step silicon nitride layer deposition by LPCVD. (c) Lithography (DUV), dry etching technique and (d) SiO_2 encapsulation by low-temperature PECVD. The details of the process flow including processing temperatures, precursors rate flows, etching chemistry and lithography are fully described in the article text.

Deposition method. The fabrication started with the 1.5-µm-thick thermal oxidation of the silicon substrate in order to provide around 3-µm-thick SiO_2 optical buffer between nitride layer and the Si substrate. The silicon nitride layer is the deposited via low-pressure chemical vapor deposition (LPCVD) in two steps, counting a 360-nm-thick layer each, tilting the carrier wafer at 45° between both depositions, each carried at 780 °C with pre-cooling around 630 °C. This as it will be shown in the measurement section prevent cracks from appearing, while providing a nitride films still exhibiting good optical properties and, most important, conserving its Kerr nonlinearity. The deposition is carried out in a vertical chamber under a 112 mTorr pressure using NH_3 and dichlorosilane (SiH_2Cl_2) as precursor gases, respectively introduced in the chamber at 200 sccm and 80 sccm flow rates. The material morphological characterization revealed a tensile strain around +1200 MPa [23].

Lithography and dry etching technique. Deep-UV (DUV) lithography was performed on a ASML-300 stepper using 248-nm DUV and 780-nm-thick M78Y resist mask followed by a 40-nm-thick anti-reflection coating (BARC). Chloride-based dry etching was used to pattern the different architectures on the Si_3N_4 film previously deposited using solely the resist as hard mask and the SiO_2 buried oxide as stop etch layer. In detail, a CF_4-CH_2F_2-O_2 chemistry was used in a 300-mm reactor under 32 mTorr pressure and 150 °C process temperature. A 20-second SiO_2 overetch was estimated to range between 20 nm and 30 nm over the full 200-mm Si wafer, while the waveguide side-wall angle was measured around 5°. An etch rate of 110 nm/minute was estimated, while an etching selectivity of the resist against the nitride layer is 1:1.5.

Encapsulation. Nitride circuits were then encapsulated by plasma-enhanced chemical vapor deposition (PECVD) of a 3-µm-thick SiO_2 cladding layer at 350 °C using SiH_4 and Ar as precursors.

In Figure 8, we showed both optical and electron scanning microscope images of the devices fabricated via the aforementioned fabrication flow.

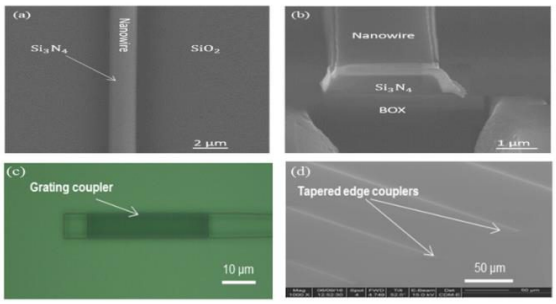

Fig. 8. Scanning electron and optical microscope images of silicon nitride fabricated devices using the aforementioned process flow as described in Section III. Scanning electron microscope (a) and focused ion beam images of Si_3N_4-based nanowires before encapsulation(b) Input/output was ensured by the presence of grating couplers (c) while tapered edge couplers featuring wider bandwidth and minor coupling losses, are included in the mask for continuum generation demonstration (d).

First, linear optical characterization was carried out in order to evaluate the linear propagation losses of the waveguides. The linear propagation loss measurements were done using an automated prober station across the whole 200-mm wafer, and light was injected via 1-dimensional grating couplers (7 dB/coupler). We derived average propagation losses of 0.3 dB/cm at 1550 nm for two-mode waveguides with cross-section dimensions ($w \times h$) of 1400 nm × 730 nm and 1.5 dB/cm for normal dispersion single-mode waveguides with cross-section dimensions of 750 nm × 730 nm. The total insertion loss of several waveguides with different lengths was measured and the propagation losses of the fundamental transverse electric polarized mode was inferred from the slope of the insertion loss as a function of the waveguide length. These results were obtained on randomly chosen dies and wafers to ensure the film to be crack-free everywhere on each 200-mm wafers. The measurements were averaged across 20 dies of different wafers. As shown in the next section, these amount of losses are sufficiently low for enabling Kerr-based self-phase modulation (SPM) in our silicon nitride nanowires under reasonable input peak powers.

Continuum generation via nonlinear Kerr SPM

Supercontinuum generation has given rise to a wide variety of research, regarding both the approaches to generate it as well as its target applications such as chemical sensing, medical imaging, or high-throughput telecommunications [19]. In fact, even moderate-bandwidth (of 60 nm) supercontinua are enough for such selected applications. We refer to these as continuum sources.

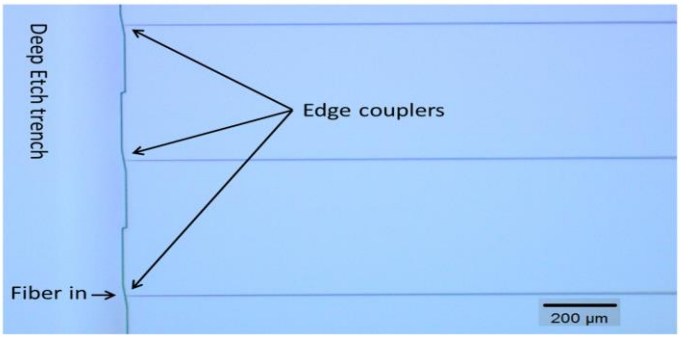

Fig. 9. Edge-coupling via inverted tapers tips of 160 nm ensuring coupling over a wide spectral window for nonlinear tests. Deep-etch trench profile (including 8° off-normal coupling facets) is to reduce feedback to fibers.

As opposed to light thermal emission, these are highly coherent. In nonlinear waveguides, the intensity-dependent refractive index leads to SPM upon the propagation of short optical pulses and the generation of spectral continuum via its Kerr nonlinearity. The equation describing the related nonlinear phase shift is as follows: $\Delta\varphi_{max} = \gamma P L_{eff}$ where P is the coupled peak power, γ is the nonlinear parameter. It is related to the nonlinear index n_2 through the expression $\gamma=\frac{\omega n_2}{cA_{eff}}$, where ω is the angular frequency, c is the speed of light and A_{eff} is the effective area The effective length L_{eff} is given by $L_{eff} = \frac{1-e^{-\alpha.L}}{\alpha}$. Depending on the linear propagation loss α, L_{eff} converges towards $L_{\max} = 1/\alpha$ as a function of the waveguide length (L). By using the measured propagation losses, we estimate L_{eff} to be 1.43 cm for our 2.1-cm-long single-mode waveguides, i.e., 56% of L_{max} (2.55 cm), meaning that by using longer waveguides we could get more SPM and a wider spectral broadening for a given input power and pulse duration. The efficiency in the continuum generation is

naturally limited by linear and nonlinear losses. In our case, the latter such as two- or three-photon absorption are negligible, as attested by the linear transmission of our waveguides, even at high pump powers.
When a pulse passes through the silicon nitride waveguide, the material intensity-dependent nonlinear index produces blue-shifted spectral components on the trailing edge and red-shifted spectral components on the leading edge of the optical pulse envelope. As the process accumulates along the waveguide, the pulse gets spectrally broadened, giving rise to a frequency continuum. Edge-coupling (1.2 dB coupling losses) via inverted tapers - as shown in figure 9 - was used in order to perform extensive nonlinear optical characterization over a large wavelength span in the 1.55 µm region. Using an external fiber-based laser followed by an erbium-doped fiber amplifier (EDFA), optical pulses of 2-ps duration with peak powers ranging from a few to hundreds of Watts at a repetition rate of 20 MHz were injected into the single-mode 2.1-cm-long silicon nitride waveguides (750 nm × 730 nm cross-section, α=1.5 dB/cm). No fusing of waveguides nor degradation of the spectral broadening over time was observed. Experimental results are illustrated in figure 10(a). As shown, by increasing the coupled peak pump power, Kerr nonlinearity can be leveraged into a SPM process capable to generate a wide-spanning continuum of new optical frequencies around the 1543 nm pump wavelength.

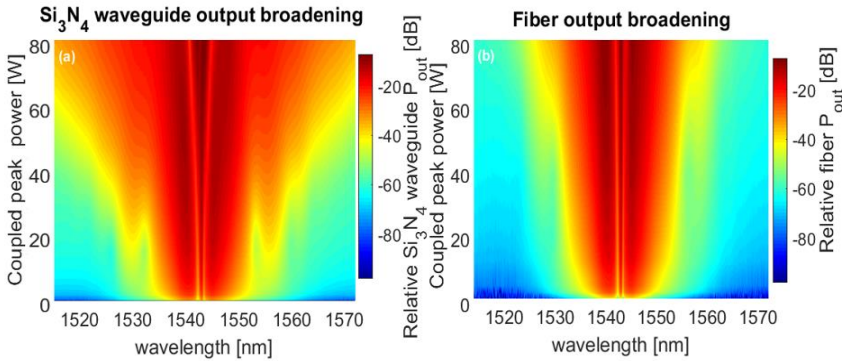

Fig. 10 - Spectral broadening of picosecond pulses via Kerr self-phase modulation (SPM) leading to the generation of a frequency continuum between 1515 - 1575 nm. (a) Spectral broadening at the Si_3N_4 waveguide output. (b) Spectral broadening measured at the fiber output (i.e., before Si_3N_4 waveguide input

IV. CONCLUSIONS AND PERSPECTIVES

In the present work authors presented the cointegration and characterization of a Si/AlGaAs supermode coupler and stoichiometric Si_3N_4-based nonlinear circuits using a process compatible with silicon photonics integrated circuits and optoelectronics. Molecular bonding is used in our process allowing the co-integration of a low-loss (<0.5 dB) link between the nonlinear AlGaAs and the Si photonics toolbox. Generation of 1515-1575 nm continuum generation is demonstrated using a silicon nitride technology which is strictly process-compatible with silicon PICs fabrication flow and thermal budgets [23].
This works paves the way toward the heterogeneous integration of nonlinear Si_3N_4-based circuits and AlGaAs continuum sources with Si optoelectronics devices and circuits. Further activities will focus on cointegration of the continuum sources with passive and active silicon photonics circuits (e.g. multiplexer, modulators).

ACKNOWLEDGEMENT

The research leading to these results has received funding from the French National program “programme d’investissment d’avenir, IRT Nanoelec, n° ANR-10-AIRT-05” and internal funding “DOPT 2020”.

REFERENCES

[1] G. T. Reed, “The optical age of silicon,” *Nature*, vol. 427, pp. 595–596, 2004.
[2] M. Asghari and A. V. Krishnamoorthy, “Silicon photonics - Energy efficient communication,” *Nat. Phot.*, vol. 5, pp. 268-270, May 2011.

[3] B. Ben Bakir, *et al.*, "Electrically driven hybrid Si/III-V Fabry-Pérot lasers based on adiabatic mode transformers," *Opt. Exp*., vol. 19, no. 11, pp. 10317–10325, 2011.
[4] M. Antelius, K. B. Gylfason, and H. Sohlström, "An apodized SOI waveguide-to-fiber surface grating coupler for single lithography silicon photonics," *Opt. Exp*., vol. 19, pp. 3592-3598, 2011.
[5] L. Liao, D. Samara-Rubio, M. Morse, A. Liu, D. Hodge, D. Rubin, U. Keil, and T. Franck, "High speed silicon Mach-Zehnder modulator," *Opt. Exp.*, vol. 13, pp. 3129-3135, 2005.
[6] L. Vivien, *et al*., "High speed and high responsivity germanium photodetector integrated in a Silicon-On-Insulator microwaveguide," *Opt. Exp*., vol 15, pp. 9843-9848, 2007.
[7] W. Bogaerts, *et al.*, "Silicon-on-insulator spectral filters fabricated with CMOS technology," *Selected Topics in Quantum Electronics, IEEE Journal of* , vol.16, no. 1, pp.33,44, Jan.-Feb. 2010.
[8] C. Sciancalepore, L. J. Richard, J.-A. Dallery, S. Pauliac, K. Hassan, J. Harduin, H. Duprez, U. Weidenmueller, D. F. G. Gallagher, S. Menezo, and B. Ben Bakir, "Low-crosstalk fabrication-insensitive echelle grating demultiplexers*," IEEE Photon. Technol. Lett.*, (*published, in press*), Dec. 04, 2014.
[9] B. Ben Bakir, A. Descos, N. Olivier, D. Bordel, P. Grosse, E. Augendre, L. Fulbert, and J. M. Fedeli, "Electrically driven hybrid Si/III-V Fabry-Pérot lasers based on adiabatic mode transformers," *Opt. Exp* 19, 10317-10325 (2011)
[10] Helene Duprez, Antoine Descos, Thomas Ferrotti, Corrado Sciancalepore, Christophe Jany, Karim Hassan, Christian Seassal, Sylvie Menezo, and Badhise Ben Bakir, "1310 nm hybrid InP/InGaAsP on silicon distributed feedback laser with high side-mode suppression ratio," *Opt. Exp* 23, 8489-8497 (2015)
[11] Thomas Ferrotti, Benjamin Blampey, Christophe Jany, Hélène Duprez, Alain Chantre, Frédéric Boeuf, Christian Seassal, and Badhise Ben Bakir, "Co-integrated 1.3µm hybrid III-V/silicon tunable laser and silicon Mach-Zehnder modulator operating at 25Gb/s," *Opt. Exp* 24, 30379-30401 (2016)
[12] J. Van Campenhout, P. Rojo-Romeo, P. Regreny, C. Seassal, D. Van Thourhout, S. Verstuyft, L. Di Cioccio, J.-M. Fedeli, C. Lagahe, and R. Baets, "Electrically pumped InP-based microdisk lasers integrated with a nanophotonic silicon-on-insulator waveguide circuit," *Opt. Exp* 15, 6744-6749 (2007).
[13] Il-Sug Chung and Jesper Mork, "Silicon-photonics light source realized by III–V/Si-grating-mirror laser," Appl. *Phys. Lett*., vol. 97, no 15, p. 151113, 2010.
[14] C. Sciancalepore, B. Ben Bakir, X. Letartre, et al., "CMOS-compatible ultra-compact 1.55-µm emitting VCSELs using double photonic crystal mirrors," *IEEE Phot.Technol. Lett.*, vol. 24, no 5, p. 455-458, 2012.
[15] J. S. Levy, A. Gondarenko, M. A. Foster, A. C. Turner-Foster, A. L.Gaeta and M. Lipson, "CMOS-compatible multiple-wavelength oscillator for on-chip optical interconnects", *Nat.Photonics*, vol. 4,pp. 37-40, 2010.
[16] Y. Okawachi, K. Saha, J. S. Levy, Y. H. Wen, M. Lipson and A. L. Gaeta, "Octave-spanning frequency comb generation in a silicon nitride chip", *Opt.Lett*, vol. 36,pp. 3398-3400, 2011.
[17] A. C. Turner, C. Manolatou, B. S. Schmidt, M. Lipson, M. A. Foster, J. E. Sharping and A. L. Gaeta, "Tailored anomalous group-velocity dispersion in silicon channel waveguides", *Opt.Exp* , vol.14, pp. 4357-4362, 2006.
[18] T. Herr, V. Brasch, J. D. Jost, C. Y. Wang, N. M. Kondratiev, M. L. Gorodetsky, & T. J. Kippenberg,"Temporal solitons in optical microresonators", *Nat.Photonics*, vol. 8, pp. 145-152, 2014.
[19] H. Hu *et al*., ―Single-Source AlGaAs Frequency Comb Transmitter for 661 Tbit/s Data Transmission in a 30-core Fiber,‖ *in proc. OSA CLEO*, pp. JTh4C-1, 2016.
[20] D. J. Moss, *et al*. , "New CMOS-compatible platforms based on silicon nitride and Hydex for nonlinear optics'', *Nat.Photonics*, vol. 7, pp. 597-607, 2013.
[21] L. Ottaviano, *et al*., "low-loss high-confinement waveguides and microring resonators in AlGaAs-on-insulator" *Opt. Lett*, vol. 41,pp. 3996-3999, 2016.
[22] K. Luke, *et al*. ,"Overcoming Si3N4 film stress limitations for high quality factor ring resonators," *Opt. Exp*., p. 22829-22833, vol. 21, no 19, 2013.
[23] H. El Dirani, *et al*.,"Crack-free silicon-nitride-on-insulator nonlinear circuits for continuum generation in the C-band," *Photon. Technol. Lett.*, vol. 30, pp. 355-358, Jan. 2018.